Solution Structure of Amyloid β-Peptide(1−40) in a Water−Micelle Environment. Is the Membrane-Spanning Domain Where We Think It Is?[†,‡]

Murray Coles,[§] Wendy Bicknell,[||] Andrew A. Watson,[§] David P. Fairlie,[§] and David J. Craik*[,§]

Centre for Drug Design and Development, The University of Queensland, Brisbane, QLD 4072, Australia, and Department of Medicinal Chemistry, Victorian College of Pharmacy, Monash University, 381 Royal Parade, Parkville, VIC 3052, Australia

Received December 3, 1997; Revised Manuscript Received May 1, 1998

ABSTRACT: The three-dimensional solution structure of the 40 residue amyloid β-peptide, Aβ(1−40), has been determined using NMR spectroscopy at pH 5.1, in aqueous sodium dodecyl sulfate (SDS) micelles. In this environment, which simulates to some extent a water−membrane medium, the peptide is unstructured between residues 1 and 14 which are mainly polar and likely solvated by water. However, the rest of the protein adopts an α-helical conformation between residues 15 and 36 with a kink or hinge at 25−27. This largely hydrophobic region is likely solvated by SDS. Based on the derived structures, evidence is provided in support of a possible new location for the transmembrane domain of Aβ within the amyloid precursor protein (APP). Studies between pH 4.2 and 7.9 reveal a pH-dependent helix−coil conformational switch. At the lower pH values, where the carboxylate residues are protonated, the helix is uncharged, intact, and lipid-soluble. As the pH increases above 6.0, part of the helical region (15−24) becomes less structured, particularly near residues E22 and D23 where deprotonation appears to facilitate unwinding of the helix. This pH-dependent unfolding to a random coil conformation precedes any tendency of this peptide to aggregate to a β-sheet as the pH increases. The structural biology described herein for Aβ-(1−40) suggests that (i) the C-terminal two-thirds of the peptide is an α-helix in membrane-like environments, (ii) deprotonation of two acidic amino acids in the helix promotes a helix−coil conformational transition that precedes aggregation, (iii) a mobile hinge exists in the helical region of Aβ(1−40) and this may be relevant to its membrane-inserting properties and conformational rearrangements, and (iv) the location of the transmembrane domain of amyloid precursor proteins may be different from that accepted in the literature. These results may provide new insight to the structural properties of amyloid β-peptides of relevance to Alzheimer's disease.

Alzheimer's disease (AD)[1] is associated with the progressive accumulation of amyloid deposits in the brain during aging and is identified by extracellular neuritic plaques and neurofibrillary tangles *(1)*. The major component of plaques is a 4 kDa peptide known as amyloid β-peptide (Aβ or βA or βA4), consisting of 39−43 amino acids with a high propensity for aggregation to form β-sheets *(2)*. Aβ is proteolytically cleaved from much larger glycoproteins known as Amyloid Precursor Proteins (APPs), which comprise 695−770 amino acids with a single hydrophobic transmembrane region and resemble glycoprotein receptors on cell surfaces (Figure 1). APPs are widely distributed in neurons and other cell types and are known to be neuroprotective *(3)*. Aβ is produced slowly in normal individuals *(4)* but more rapidly in people having amyloidogenic (e.g., AD) or certain other genetically related diseases (e.g., Down's syndrome) and following brain injuries, where there is overexpression of APPs. A causal relationship between Aβ and the development of AD has not been conclusively demonstrated *(5)*, and the peptide may instead be a consequence of the disease. Nevertheless, Aβ is neurotoxic in the aggregated fibrillar form *(6−8)*, and this may be an important clue to its role in AD. A better understanding of the formation, structure, aggregation, and neurotoxic action of Aβ may facilitate the development of therapeutic agents for the treatment of AD. Here we report the use of NMR spectroscopy to determine the solution structure of Aβ(1−40) in a water−micelle environment.

The 40 residue peptide Aβ(1−40) is the major Aβ sequence (90%) found circulating in cerebrospinal fluid, while Aβ(1−42) and other lengths are minor components *(9, 10)*. On the other hand, the major component of plaques is Aβ(1−42) with smaller amounts of Aβ(1−40) *(2, 11)*. It has been suggested that Aβ(1−42) may seed the aggregation

[†] This work was supported by the National Health and Medical Research Council of Australia. D.J.C. is an Australian Research Council Senior Fellow.

[‡] Coordinates have been deposited in the Brookhaven Protein Data Bank under ID code 1BA4.

* To whom correspondence should be addressed (Fax, +61-7-3365-2487; telephone, +61-7-3365-4945; Email, d.craik@mailbox.uq.edu.au).

[§] The University of Queensland.

[||] Monash University.

[1] Abbreviations: Aβ, amyloid β-peptide; APP, amyloid precursor protein; NMR, nuclear magnetic resonance; SDS, sodium dodecyl sulfate; AD, Alzheimer's disease; TFA, trifluoroacetic acid; DIPEA, *N*, *N*-diisopropylethylamine; DMF, *N*,*N*-dimethylformamide; DNP, 2,4-dinitrophenyl; HPLC, high-performance liquid chromatography; Boc, *tert*-butyloxycarbonyl; PAM, phenylacetamidomethyl; ESMS, electrospray mass spectrum; TOCSY, total correlation spectroscopy; NOESY, nuclear Overhauser enhancement spectroscopy; DQF-COSY, double quantum filtered correlation spectroscopy; DQ, double quantum; TFE, 2,2,2-trifluoroethanol; LiDS, lithium dodecyl sulfate; ApoE, apolipoprotein E; CD, circular dichroism.

S0006-2960(97)02979-6 CCC: $15.00
Published on Web 07/16/1998

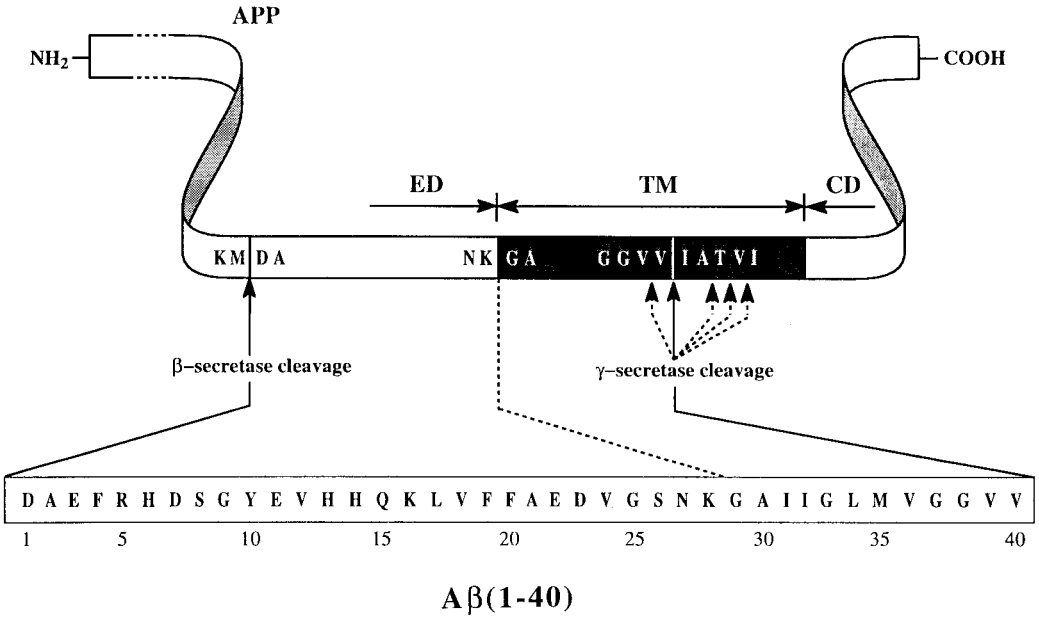

FIGURE 1: Processing of APP to form Aβ. The intact protein is proposed to consist of an extracellular domain (ED), a transmembrane domain (TM, shaded box), and a cytoplasmic domain (CD). The β- and γ-secretase cleavage sites are indicated by arrows, with dashed arrows showing alternative γ-secretase sites. A dashed line shows the position of the putative membrane boundary relative to the Aβ(1−40) sequence.

Table 1: Summary of Solution NMR Structural Studies of Aβ Peptides

peptides studied	concn, solvent, pH, temp	main stuctural features	ref
Aβ(1−28)	3.5 mM, TFE/H_2O 6:4,	helical segment 10/11−26, also less well-defined helix 2−6	(*49*)
Aβ(1−28)	4.1 mM, TFE/H_2O 6:4, pH 1−4, 283−308 K	pH 1, 283 K fully helical; as pH and temperature increase helix unfolds into two helical regions, 2−7 and 10−27; at 308 K, helix 2−7 becomes random coil while 13−20 remains helical	(*33*)
Aβ(1−28) and Aβ(1−28[E22Q])	2−2.9 mM,DMSO, 298 K	both have flexible N-terminus and well-defined C-terminus, 16−28, with helical segment and turn-like structure; native has well-defined helix between 21−24; mutant is helical between 17−24	(*35*)
Aβ(1−28)	2 mM, SDS micelles, pH 3, 298 K	two helices, 2−11 and 13−27, connected via bend at Val12	(*34*)
Aβ(12−28)	TFE/H_2O 6:4, pH 2.4	partially helical	(*50*)
Aβ(10−35)NH_2 and Aβ(1−28)	250−300 μM, H_2O, pH 2.1 and 5.6, 283 K	at pH 5.6, Aβ(10−35)NH_2 is not helical but suggests several turns and at least 2 short strands; Aβ(1−28) is not helical at pH 5.6	(*14*)
Aβ(1−40)	2.5 mM, TFE/H_2O 4:6, pH 2.8, 298 K	two helices, 15−23 and 31−35; the rest was random coil	(*32*)
Aβ(25−35)	2 mM, LiDS micelles, pH 4, 308 K	short C-terminal helical region	(*42*)
Aβ(12−28)	3 mM, SDS micelles, pH 5.6, 303 K	residues 16−24 are helical	(*29*)

and deposition of other Aβ peptides *(12)*. Small fragments of Aβ(1−42), for example, Aβ(25−35) *(13)*, are known to form fibrils in vitro. Lee et al. *(14)* found that Aβ(1−28) was not plaque-competent at any pH tested, while Aβ(10−35)NH_2 and Aβ(1−40) were plaque-competent but only in the pH range 5−9. Burdick et al. *(15)* have shown a similar relationship between fibril formation and pH in an in vitro assay and also demonstrated that longer peptides are able to form fibrils over a wider range of pH, Aβ(1−42) forming fibrils at pH >7.4 whereas shorter peptides such as Aβ(1−39) do not form fibrils in this pH range.

Since there have been several differing reports of the solution structures of Aβ fragments using a wide variety of techniques and experimental conditions (Table 1), it is difficult to draw conclusions about the physiologically relevant solution structure of Aβ(1−40) or Aβ(1−42). Because they are less prone to aggregation, smaller fragments of these peptides have generally been studied in aqueous acid or TFE solutions which bear little relationship to physiological conditions. As the C-terminus of Aβ(1−40), namely, residues 29−40, is thought to be inserted in membrane while incorporated within APP *(16)*, we decided to examine the three-dimensional solution structure of Aβ(1−40) in water/sodium dodecyl sulfate (SDS) micelles because of their widespread use to simulate a water−membrane interface *(17)*. Aβ(1−40) is soluble in micelles, simulating to some extent a cell membrane environment. This water−micelle medium has also allowed us to study the effects of pH on peptide conformation. This study is aimed at providing a better understanding of conformational changes that precede

aggregation of Aβ peptides, and toward developing viable strategies for inhibiting aggregation.

MATERIALS AND METHODS

Synthesis of Aβ(1−40). The following chemicals were purchased from Auspep, Melbourne, Australia: trifluoroacetic acid (TFA), *N*,*N*-diisopropylethylamine (DIPEA), and *N*,*N*-dimethylformamide (DMF). Protected amino acids were purchased from Calbiochem-Novabiochem, Sydney, Australia, and Applied Biosystems, Brisbane, Australia. Acetonitrile (HPLC grade) was purchased from BDH, Poole, England. Other chemicals and solvents were of reagent grade. The Boc-Val-PAM resin (0.77 mmol g^{-1}) was purchased from Applied Biosystems, Brisbane, Australia. Electrospray mass spectra were recorded on a P E SCIEX API III triple-quadrupole mass spectrometer.

Preparative reverse-phase HPLC was performed on a Waters Delta-Pak PrepPak C_{18} cartridge (40 mm × 100 mm, 100 Å) using a Waters Delta Prep 4000 preparative chromatography system. Analytical runs were performed similarly but on a Waters Delta-Pak Radial-Pak C_{18} 8 mm × 100 mm cartridge. Elution profiles were monitored at 214 nm.

The peptide was prepared manually by solid-phase peptide synthesis using Boc-Val-PAM resin and Boc-chemistry protocols *(18)*. The DNP side chain protecting groups on the histidine residues were removed prior to cleavage by reaction with DIPEA and mercaptoethanol in DMF (1:2:7, 2 × 30 min). The peptide was deprotected and cleaved from the resin using anhydrous liquid hydrogen fluoride, *p*-cresol, and *p*-thiocresol (10 mL, 9:0.5:0.5) at 269−271 K for 70 min. The crude peptide was washed with diethyl ether under nitrogen and purified by preparative reverse-phase HPLC, using 0.1% TFA as initial eluent, this being diluted by 90% acetonitrile/0.1% TFA on a linear gradient over 70 min: ESMS calcd for $(MH)^+$ $C_{194}H_{296}N_{53}O_{58}S$, 4330.9; found $(MH)^+$, 4330.8.

Sample Preparation. For NMR studies, two samples of Aβ(1−40) were prepared with a peptide concentration of 1 mM. One sample contained the peptide dissolved in 100 mM sodium dodecyl-d_{25} sulfate (SDS) in 90% MilliQ H_2O and 10% D_2O at pH 5.1, the pH measurement being uncorrected for isotope effects. A second sample was made up containing 1 mM Aβ(1−40) and 100 mM SDS in 100% D_2O; the pH of this sample was adjusted, using small aliquots of 0.01 M DCl or NaOD, for use in pH studies (uncorrected meter readings were recorded). Both samples remained stable in solution for several months at room temperature.

NMR Experiments. ^{1}H NMR spectra of the Aβ(1−40) peptide were acquired at 500, 600, and 750 MHz on Bruker AMX-500, DRX-500, AMX-600, and DRX-750 spectrometers. All data were collected at 298 K, with repetition of some experiments at 310 K for the sample containing SDS in 90% H_2O. NOESY *(19)*, TOCSY *(20)*, and DQF-COSY *(21)* spectra were acquired on all samples, with a DQ spectrum also recorded on the sample in SDS/D_2O solution. All two-dimensional spectra were collected using either 2048 or 4096 complex data points in F2, acquiring 256−400 increments in F1 for the TOCSY and NOESY and 500−700 increments for the DQF-COSY and DQ spectra. Spectra were acquired in the phase-sensitive mode using time-proportional phase incrementation for quadrature detection in the t_1 dimension *(22)*.

For the SDS/90% H_2O sample, the solvent signal was suppressed either by low-power presaturation during the relaxation delay (DQF-COSY and DQ spectra) or by the use of pulsed field gradients *(23)* (TOCSY and NOESY spectra). The quality of TOCSY spectra was poor at a mixing time of 80 ms, normally used for peptides of this size, but was slightly improved at shorter mixing times (40−60 ms), consistent with there being strong association of the peptide with high molecular weight SDS micelles. NOESY data were collected with a mixing time of 150 ms. Studies of the effect of pH were carried out in SDS/D_2O solution at 750 MHz. TOCSY spectra (40 ms mixing time) were acquired at 298 K at pH values of 4.2, 5.1, 5.8, 6.4, 6.9, and 7.9. NOESY spectra (150 ms mixing time) were also acquired at pH values of 5.1, 6.4, and 6.9 and DQ spectra (evolution time 17 ms) at pH 4.2 and 6.9. An additional NOESY spectrum (150 ms mixing time) was acquired at 500 MHz for the sample at pH 7.9. The rate of disappearance of amide proton signals on dissolution of the peptide in SDS/D_2O (pH 5.1) was monitored to assess their degree of protection from solvent. 1D spectra taken from 5 to 20 min after dissolution and 2D spectra (NOESY and TOCSY) recorded over the subsequent 24 h were used to identify slowly exchanging amides.

Spectral data were processed on a Silicon Graphics Indy computer using standard Bruker software (XWINNMR Version 1.2). In some cases, noise in the TOCSY and NOESY spectra was diminished by processing only the first 1024 complex points in F2. Data were zero-filled to 4096 points in F2 and to 1024 points in F1 and then transformed with a sine-bell squared window function shifted by between $\pi/2$ and $\pi/3$ as appropriate. Base line correction was carried out on either side of the residual water signal. For the DQF-COSY, the window function was an unshifted sine-bell. To measure coupling constants, sections of the spectra were zero-filled to 8K points prior to transformation. Spectra were internally referenced to the HDO peak according to the method of Wishart et al. *(24)*.

Structure Calculations. The 150 ms NOESY spectrum of the H_2O/SDS solution (600 MHz, 298 K, pH 5.1) was used for the extraction of distance restraints for use in quantitative structure calculations. All cross-peaks which could be assigned unambiguously were classified according to their intensity, as judged by counting cross-peak contours. Four categories were defined (strong, medium, weak, and very weak) which resulted in restraints on the upper-limit of proton separations of 2.8, 3.4, 4.2, and 5.0 Å, respectively, with allowances for the use of pseudo-atoms where appropriate. Some additional data were included after examining the NOESY spectrum at 750 MHz (D_2O/SDS solution, 298 K, pH 5.1) where the extra resolution allowed ambiguities in the 600 MHz spectrum to be resolved. Hydrogen bond distance restraints were also included for amide protons which exchanged slowly in D_2O and where a hydrogen bond acceptor had been consistently predicted in preliminary structure calculations. In these cases, the distance between the amide proton and the receptor carbonyl oxygen was restrained to 1.58−2.30 Å and that between the amide nitrogen and the carbonyl oxygen to 1.58−3.20 Å. Some information on the predominant rotamers of several side

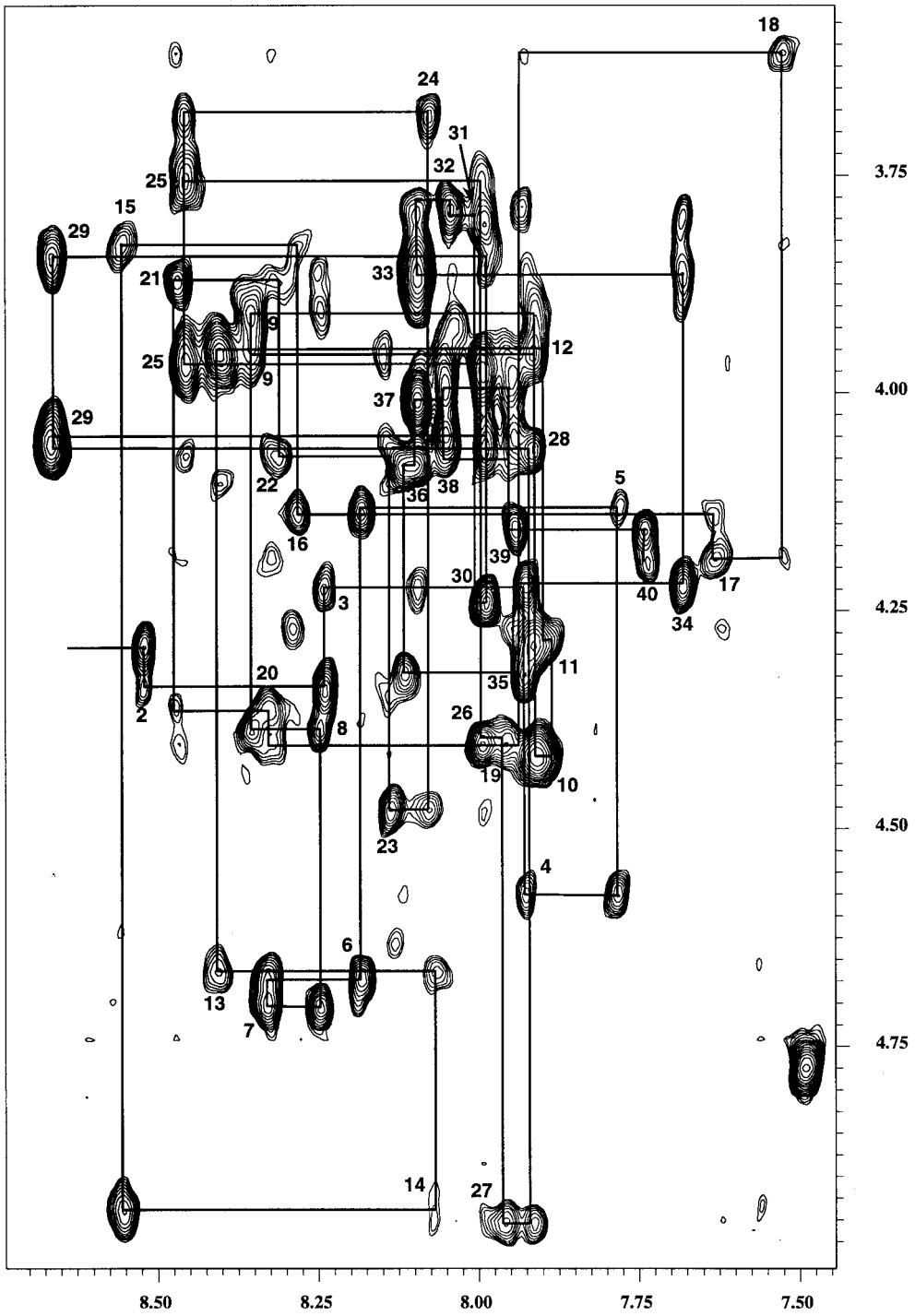

FIGURE 2: Hα−HN fingerprint region of the 150 ms NOESY spectrum of Aβ(1−40) in SDS/H_2O solution (600 MHz, pH 5.1, 298 K). The sequential assignment of all residues is indicated, with intraresidue Hα−HN cross-peaks numbered.

chains was available from $^3J_{H\alpha-H\beta}$ coupling constants and NOESY cross-peak patterns. This information was included in structure calculations using dihedral restraints.

Structure calculations were carried out in XPLOR *(25)* using simulated annealing and with both distance and dihedral restraints applied using standard XPLOR potential wells and force constants. A three-stage procedure was followed. First, simulated annealing calculations were carried out using the protocol sa.inp (30 ps of dynamics at 2000 K followed by 16 ps of dynamics during which the system was cooled linearly to 50 K) generating sets of 20 structures. Each of these structures was then treated to a simulated annealing based refinement stage (refine.inp; 16 ps of dynamics during which the temperature was ramped linearly from 1000 to 50 K) which places higher emphasis on experimental restraints. Finally, the structures were minimized (4000 steps using the Powell algorithm) in a modified version of the XPLOR force field "PARMALLH3X.PRO". This force field had been modified such that dihedral terms about rotatable bonds had been removed, allowing 1−4 nonbonded interactions to be calculated explicitly (i.e., NBXMOD = 5). Angular order parameters and pairwise RMS deviations were calculated for the final structure set using XPLOR macros written for the purpose. The calculated structures were examined visually

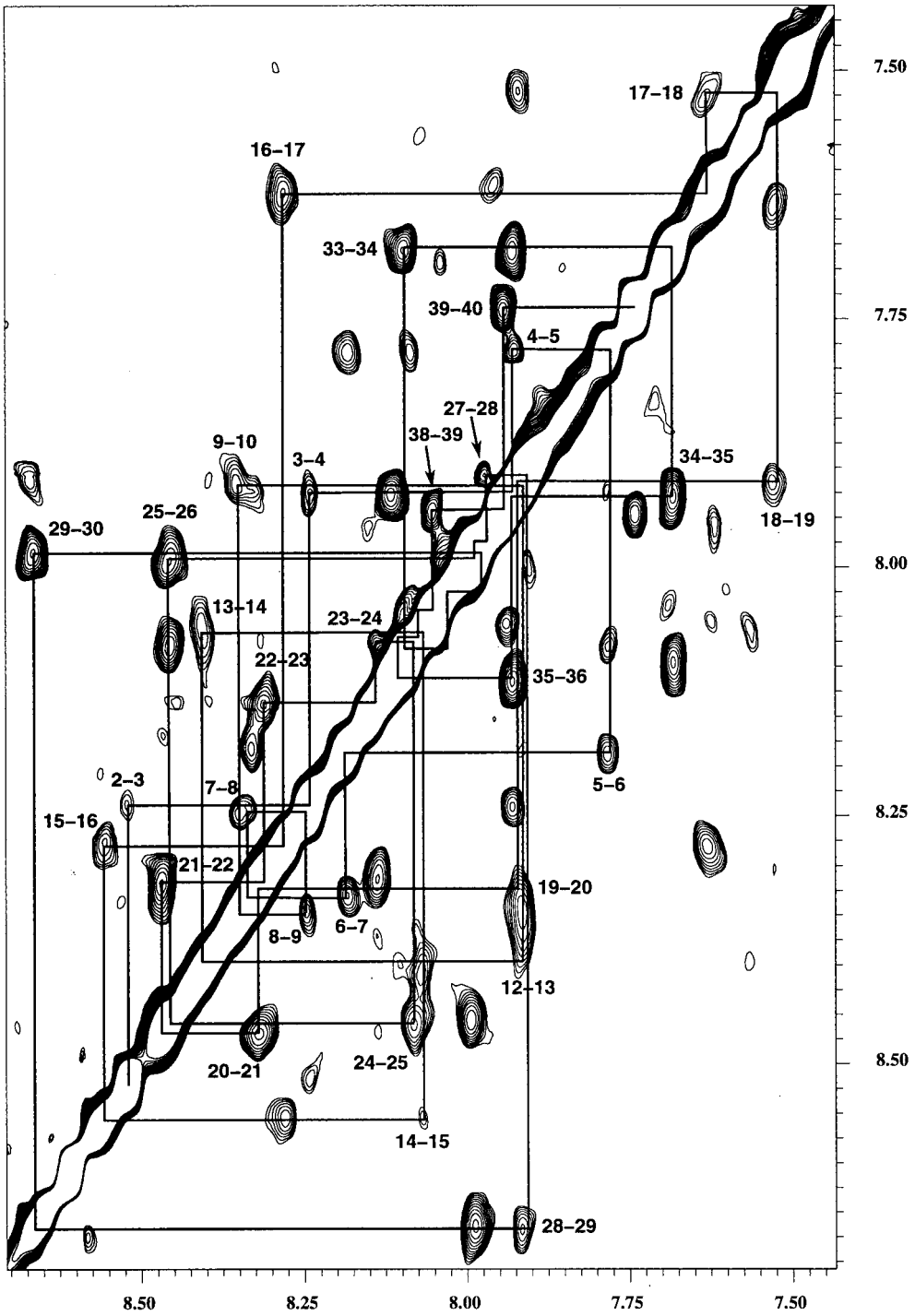

FIGURE 3: HN−HN region of the NOESY spectrum of Aβ(1−40) in SDS/H_2O solution (600 MHz, pH 5.1, 298 K). Sequential HN−HN connectivities are observed for all residues, and these are indicated. The high intensity of many of these connectivities is consistent with the presence of helical structures.

using the InsightII molecular graphics program of Biosym/MSI.

RESULTS

Aqueous SDS Solution. Aβ(1−40) was soluble at millimolar concentrations in aqueous 100 mM SDS and yielded 1D and 2D NOESY NMR spectra of good quality. There was no evidence of gelling or precipitation of the sample over several weeks, and the spectra did not change over this period. This suggests that the peptide did not aggregate in the water/SDS micelle solution. The TOCSY spectra were generally of poorer quality than the NOESY spectra. This has been observed previously in studies of certain peptide−micelle mixtures *(26)* and is consistent with strong association of peptide molecules with SDS micelles, the high molecular mass of the complex resulting in poor magnetization transfer in TOCSY spectra. Assuming there are 60−70 SDS monomer units per micelle *(17)*, the molecular mass of the Aβ(1−40)/SDS−micelle complex is >20 kDa, consistent with poor TOCSY but excellent NOESY spectra.

The majority of resonances were assigned using standard sequential assignment techniques, although some ambiguities

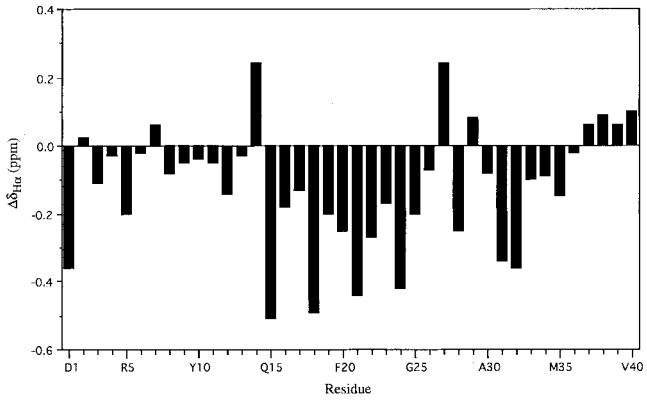

FIGURE 4: Differences of α-proton chemical shifts from random-coil values ($\Delta\delta_{H\alpha}$) for Aβ(1−40) in SDS/H_2O solution at pH 5.1 and 298 K. The random-coil values of Andersen et al. *(48)* were used. Groups of $\Delta\delta_{H\alpha}$ values less than −0.1 ppm, such as those between residues 15 and 25 and 31 and 35, can be correlated with helical structures.

remained after examining TOCSY and NOESY spectra. These ambiguities were resolved by DQF-COSY and DQ spectra in D_2O/SDS solution, the latter being particularly useful for assigning resonances from glycine residues and aromatic side chains. Figure 2 shows the fingerprint region of the 600 MHz NOESY spectrum (298 K, pH 5.1) and indicates sequential assignments for all residues. Figure 3 shows the HN−HN region of the NOESY spectrum.

The measured Hα-proton chemical shifts were first compared with random coil shifts, shown as a difference plot ($\Delta\delta_{H\alpha}$) in Figure 4. Deviations of more than −0.1 ppm from random coil are usually associated with helical structures. The plot shows negative $\Delta\delta_{H\alpha}$ values for two groups of residues, Q15 to G25 and A30 to M35, indicating that they may be in a helical conformation. Since the Hα-protons of H14 and N27 are shifted downfield and have high positive $\Delta\delta_{H\alpha}$ values, they are unlikely to be involved in a helix; in the case of N27, this indicates that any helix is not continuous from Q15 to M35, but may be broken into two halves. This possibility was further investigated by examining the observed NOE connectivities.

Analysis of the NOESY spectra provided 147 intraresidue, 108 sequential, and 83 medium-range connectivities as summarized in Figure 5. There are a large number of connectivities (55) with a range of three residues, the majority being of the type $\alpha\beta(i,i+3)$ and αHN$(i,i+3)$. All of these fall within the region spanning L15 to G37. Also, several connectivities with a range of four residues were observed over this region. The combination of numerous connectivities with a range of three and four residues and intense sequential HN−HN connectivities is strong evidence of a helical structure over residues 15−37, consistent with the above analysis of $\Delta\delta_{H\alpha}$ values. The lack of medium-range cross-peaks for the N-terminal region of the molecule (residues 1−14) is indicative of a lack of well-defined secondary structure in this region. No connectivities of range greater than four residues were observed, indicating that the N-terminal region is not closely associated with the C-terminal helical region.

A feature of the NOE connectivities summarized in Figure 5 is the small stretch of residues from G25 to G29 for which medium-range NOE connectivities expected for a helix either are of low intensity or are not observed. Careful analysis of the NOESY spectra shows that these connectivities are not hidden by spectral overlap, consistent with a break in the helix suggested by the positive $\Delta\delta_{H\alpha}$ for N27. Figure 5 also shows that amide protons for residues 17−24 and 30−37 slowly exchange in D_2O, while those for residues 25−29 exchange rapidly. This is strong evidence for two independent helices, with a discontinuity over residues 25−29. The presence and nature of this discontinuity were investigated further by carrying out quantitative structure calculations.

The distance restraints used in the quantitative analysis were finalized after carrying out stereospecific assignments,

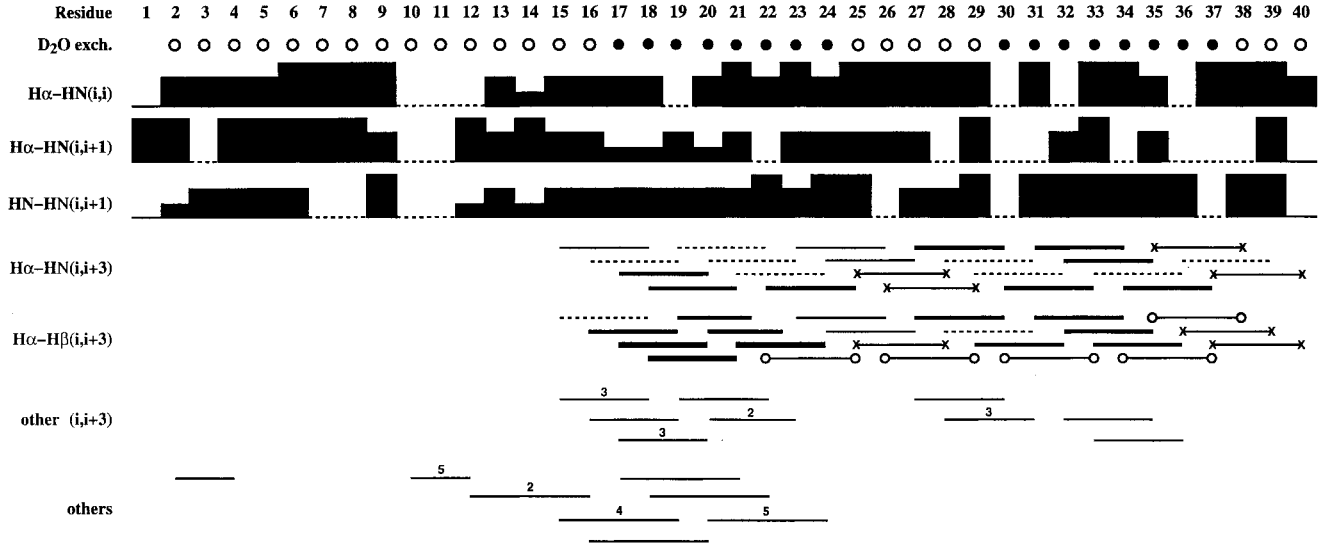

FIGURE 5: NOE connectivities observed for Aβ(1−40) at pH 5.1 and 298 K. The strength of connectivities is indicated by the height of the boxes and thickness of lines. Dashed lines indicate where cross-peak intensities could not be measured due to spectral overlap while lines with crosses indicate where a connectivity is definitely absent (i.e., no cross-peaks were detected, and the relevant spectral region is not overlapped) and lines with circles indicate where the connectivity is not applicable to the residue type. For medium-range NOEs where only the residues and not the specific protons are given, the number of connectivities observed between the two residues is indicated above the line. The D_2O exchange properties of amide protons are also shown, with those exchanging slowly enough to give cross-peaks in 2D spectra recorded within 24 h of dissolution marked with filled circles.

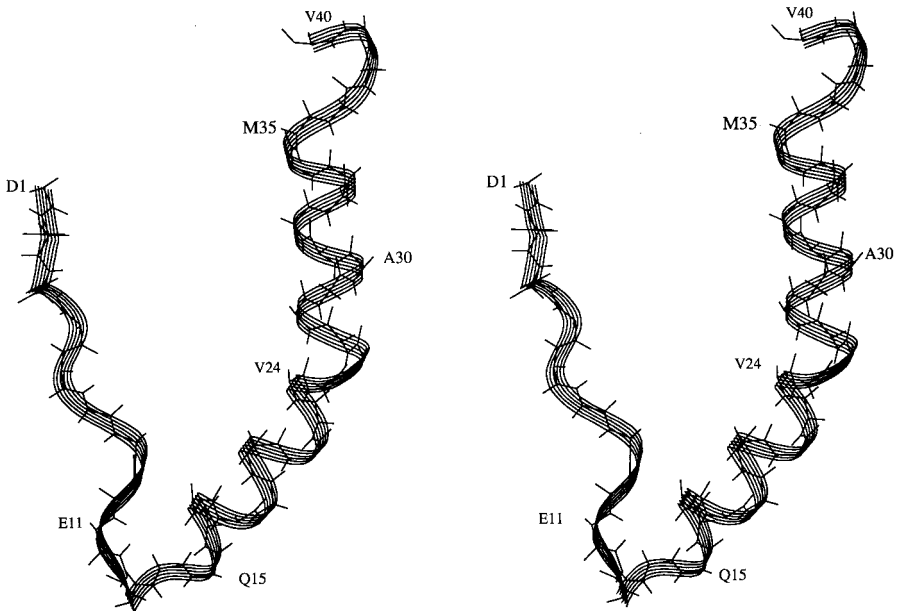

FIGURE 6: Stereoview of a typical structure calculated for Aβ(1−40). All backbone atoms and an α-carbon ribbon are shown. The helical nature of the C-terminal two-thirds of the molecule is clear, although the helix is kinked in the region of residues 26−28.

available for the prochiral Hβ protons of five AMX residues (H6, D7, H14, D23, and N27) and for the prochiral methyl groups of four valine residues (V12, V18, V24, and V36). Those prochiral groups which had not been assigned were replaced with pseudo-atoms, leaving 127 intraresidue, 100 sequential, and 80 medium-range distance restraints for use in structure calculations. Hydrogen bond restraints were included for amide protons of residues 18−24 and 31−37. In each case, the H-bond acceptor was the carbonyl oxygen in the (i−4) position which was clearly identified in a preliminary set of calculations which did not include hydrogen bond restraints. No restraint was used for the two slowly exchanging amide protons, residues 17 and 30, for which no acceptor was found in the preliminary calculations.

Dihedral restraints were also included in calculations. Due to the broad line widths for aqueous SDS solutions, destructive interference of antiphase components of cross-peaks in the DQF-COSY spectra precluded accurate measurement of $^3J_{H\alpha-NH}$ coupling constants. However, some information was available on side chain conformations of AMX and valine residues. Dihedral restraints were applied to the side chain χ1 torsion angle where the predominant rotamer was indicated during the process of stereospecific assignment. The restraints used for AMX residues were 60° for D7, 180° for D23, and −60° for H14 and N27. Those for valine residues were −60° for V12 and 180° for V18, V24, V39, and V40 (±30° in each case).

Structure Calculations. The structure calculation protocol yielded a set of 20 structures for Aβ(1−40), 1 being removed due to high violations of experimental restraints. None of the 19 remaining structures violated more than 3 restraints by >0.3 Å, and the majority had 1 or no violations at this threshold. Also, no distance restraint was violated consistently across the structure set. Similarly, for dihedral restraints, most structures had one or no violations. Thus, the structures show very good agreement with the experimental data.

Figure 6 shows a single structure calculated for Aβ(1−40). The helical nature of the C-terminal two-thirds of the molecule (residues 15−36) is clearly shown. As predicted by qualitative analysis, residues 25−27 form a kink in the helix which may represent a "hinge" region between the two helical components. Some care is needed in analyzing the nature of this region to determine whether it has any well-defined structure or whether it is a region of mobility. These issues were addressed by calculating angular order parameters for the structure set and by superimposing various regions and structure subsets.

Angular order parameters, calculated for the final structure set for the backbone torsion angles ϕ and ψ of all residues, are shown in Figure 7. High order parameters, indicating well-defined torsion angles, are generally observed within the helical region between the ϕ angle of Q15 and the ψ angle of V36. However, slightly lower values are observed for the kinked region, particularly for the angle of S26, serine being a well-known helix breaker. The lack of well-defined structure in this region suggests that the helix can best be regarded as two separate regions, namely, 15−24 and 28−36. Other regions of the molecule also show generally lower order parameters. The molecule can therefore be divided into five regions: the N-terminus (residues 1−14), helix 1 (15−24), "kink" (25−27), helix 2 (28−36), and C-terminus (37−40). Further structural analysis and calculation of RMS deviations were carried out for these regions.

Superimpositions over backbone atoms allowed calculation of average pairwise RMS deviations of structures within sets. Over the whole molecule the RMSD for backbone atoms was 5.70 Å, an understandably high figure given the unstructured nature of regions of the peptide. When backbone superimposition was carried out over the well-defined regions only, the RMS deviations were 0.20 and 0.14 Å, respectively, for helix 1 (15−24) and helix 2 (28−36), indicating very good agreement between structures. Figure 8 shows the results of the superimposition over helix 1 with the backbones of all residues shown and α-carbon ribbons drawn over residues 15−36. The helical structure of both regions is clearly demonstrated, and the range of orientations of the two helices relative to each other is also clear.

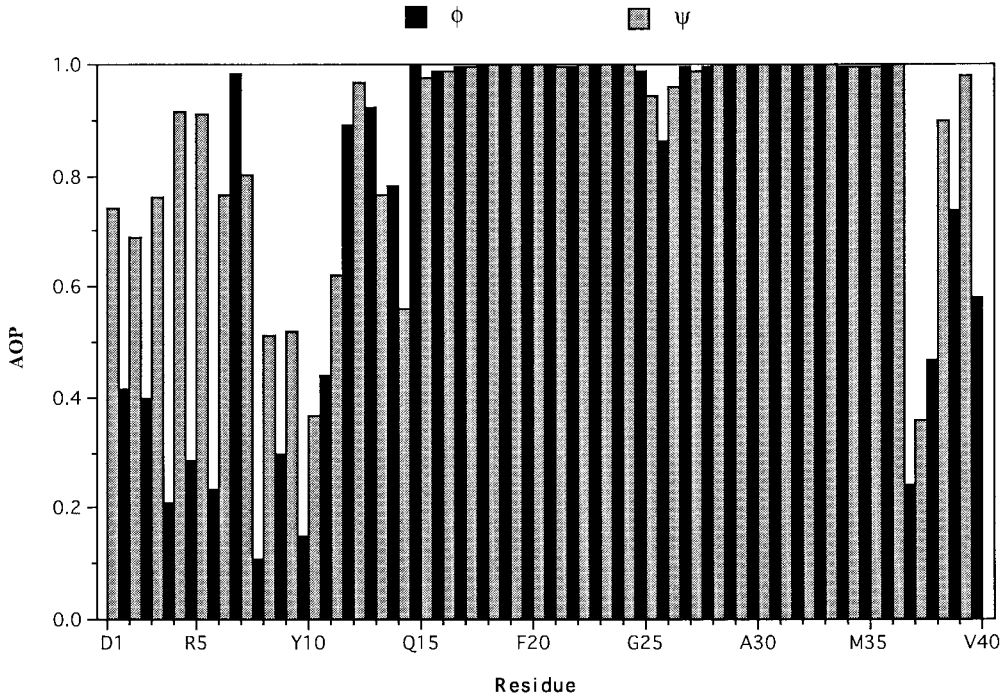

FIGURE 7: Angular order parameters calculated over the final structure set for the backbone angles ϕ and ψ of all residues. Order parameters approach 1.0 where angles are very well-defined.

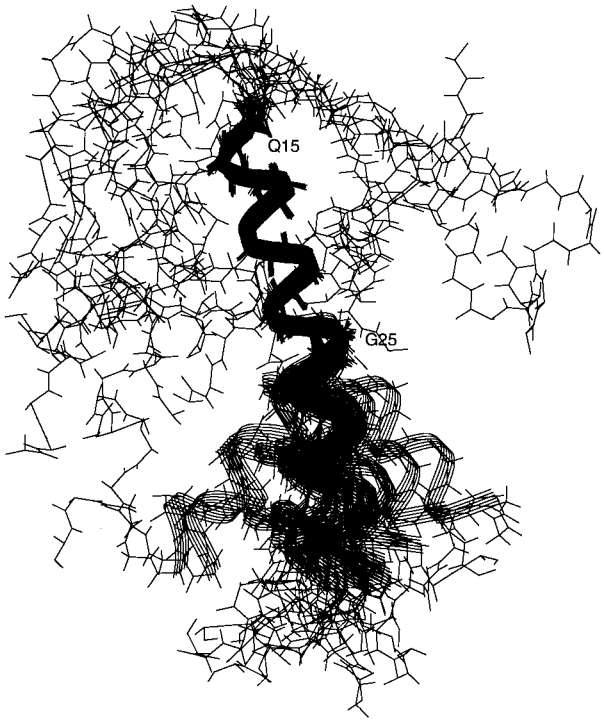

FIGURE 8: Superimposition of all structures in the final structure set over residues 15−24. All backbone atoms are shown, and an α-carbon ribbon is shown for residues 15−36. The superimposed residues form a well-defined helix. The helical nature of residues 28−36 is also shown. However, the orientation of the two helices relative to each other varies.

Superimposition of the structures over residues 15−36 gave an RMSD of 1.44 Å, and superimposition over residues 15−24 and 28−36 gave 1.37 Å.

To investigate whether certain orientations of the two well-defined regions were favored, either by force field energy terms or by experimental restraints, subsets of structures were created. These subsets contained five structures with the lowest restraint energy or the lowest total energy (excluding restraint energy). RMSD values for the superimposition of these subsets over residues 15−36 did not differ significantly from that for superposition of all structures. For example the lowest RMSD, obtained for the five structures with the lowest total energy, was 1.12 Å. Thus, no orientation is preferred in sets of low energy structures or in those which best obey experimental restraints.

Alternatively, structures can be grouped into conformational families. When RMSD values were tabulated for all pairwise superimpositions over residues 15−36, the majority of structures were related to fewer than two others at a threshold of 1.0 Å. Thus, the structures tend to be spread evenly over a range of orientations. This is also reflected in the "kink" angle (θ) as defined by the interaxial angle for axes through the backbone atoms (Cα, C═O, N) of the two helices *(27)*. The structures vary from slightly kinked (θ = 29°) to severely kinked (θ = 76°), with an average kink angle of 48° and standard deviation of 15°. The NOE data reveal that neither of these extremes represents a persistent solution structure; the medium-range (i,i+3) connectivities expected for the least kinked structure, e.g., S26Hα−G29HN, are absent, while connectivities between side chains such as V24−I31, expected in the severely kinked conformer, are also absent. The experimental data are consistent with the interpretation that the molecule is in motion between these two extremes, and so the kinked region may act as a mobile hinge with no preferred orientation for the two well-ordered helical regions.

It is interesting that helix 2 is composed entirely of hydrophobic residues, except for a single lysine at the beginning, but helix 1 has amphipathic character. One face of helix 1 contains only hydrophobic residues (Val, Ala, Leu, and Phe) while the other has three charged residues (Glu, Asp, and Lys) together with Gln and Phe. This has

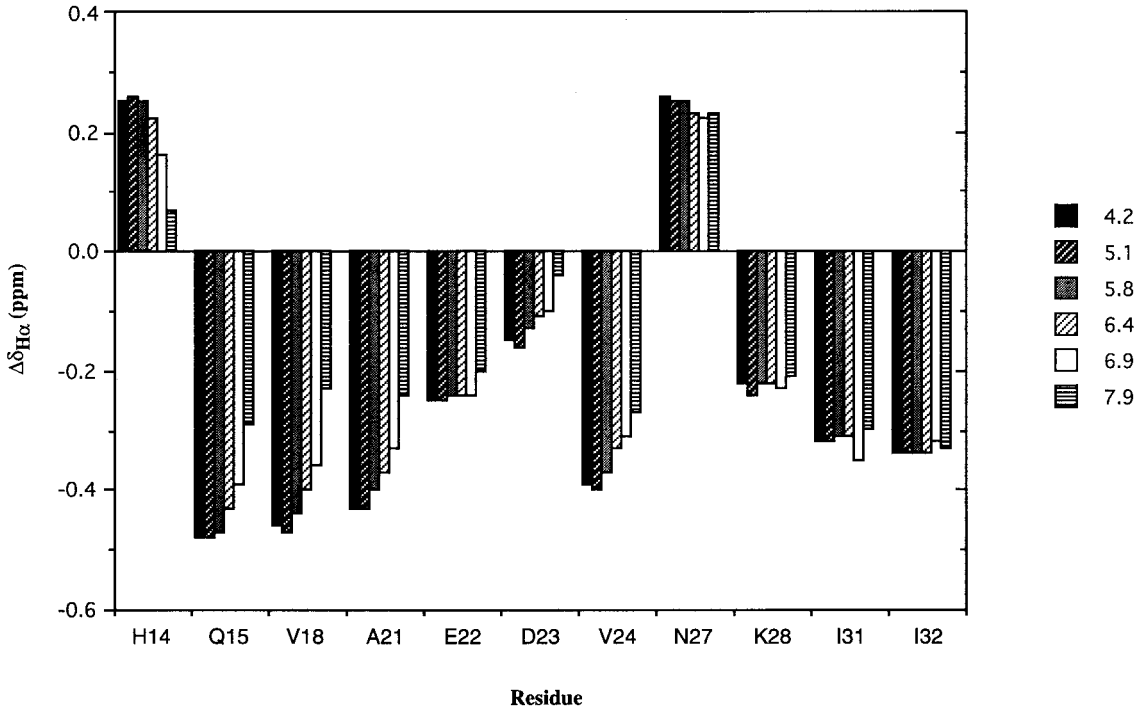

FIGURE 9: Conformational changes with pH monitored by differences from random- coil chemical shifts. The differences of the α-proton chemical shift from random coil values ($\Delta\delta_{H\alpha}$) are shown for five pH values as indicated on the figure. A selection is shown of nine residues which have large $\Delta\delta_{H\alpha}$ values at low pH. Also, values for E22 and D23 are included as these have side chains shown to titrate over this pH range (see Figure 10). In general, α-proton chemical shifts tend toward random-coil values as the pH is increased for residues in the range 14−24, while those for residues 27−32 are less pH-sensitive.

significant implications for association of Aβ with membranes (see Discussion).

The two termini form unstructured regions of the molecule. The C-terminal region is small, consisting of residues 37−40, and adopts a generally extended conformation. The pairwise RMSD for superimposition over these residues is 1.09 Å. The unstructured region at the N-terminus, however, constitutes more than one-third of the peptide, spanning residues 1−14, of which 10 are hydrophilic. The pairwise RMSD for superimposition over this region is 3.76 Å. Although there are no recognizable elements of secondary structure in this region, most structures show a turn centered on V12 and H13, which tends to orient an extended strand spanning residues 1−12 antiparallel to the 15−24 helix. The exact nature of this turn is not well-defined by the data due to extensive resonance overlap of the residues involved, especially the amide protons of Y10, E11, and V12.

pH Studies. The effects of pH on conformation were investigated by acquiring a series of spectra over the range 4.2−7.9. Changes in conformation over this range were assessed by analyzing differences of Hα chemical shifts from random coil values ($\Delta\delta_{H\alpha}$). In general, chemical shifts were closer to random coil values at higher pH, indicating that the peptide becomes less structured as the pH increases. Figure 9 shows a plot of $\Delta\delta_{H\alpha}$ versus pH for a selection of residues with large $\Delta\delta_{H\alpha}$ values at low pH. This graph clearly shows that residues in and immediately preceding helix 1 show the largest changes in $\Delta\delta_{H\alpha}$ with increasing pH. Other residues, including residues 27 and 28 in the hinge region and residues 31 and 32 in helix 2, show little change. This establishes that the helicity of the 15−24 region is selectively sensitive to pH. More direct conformational evidence of the unfolding of helix 1 comes from the strength of NOE connectivities in the region, changes in the intensity of $\alpha\beta(i,i+3)$ NOEs being diagnostic of helicity. In the spectra at pH 7.9 these connectivities are lower in intensity than at pH 5.1. Thus, it can be concluded that helix 1, particularly its C-terminal end, is more susceptible to unfolding with increasing pH than helix 2.

The unfolding of helix 1 was investigated further by monitoring the pH dependence of chemical shifts for residues with charged side chains (Figure 10). The pH behavior of E22 and D23 in the upper panel and the behavior of H14 in the lower panels are clearly quite different from other residues of similar type. Although E22 and D23 would normally have pK_a values of ca. 4.5, the greatest chemical shift changes for these residues occur at pH 6−7, indicative of higher pK_a. These apparently higher pK_a values are not due to formation of salt bridges, which would be expected to depress pK_a values, but are likely to be due to interaction of the peptide with the micelle *(28, 29)*.

DISCUSSION

In the current study, the structure of Aβ(1−40) has been determined in the presence of SDS micelles. Given that the SDS concentration was 100-fold higher than that of Aβ(1−40) and that there are 60−70 SDS molecules per micelle, the solution contains an excess of micelles over Aβ(1−40) molecules. The NMR data and physical characteristics of the sample [i.e., nongelling after several weeks relative to rapid gelling of Aβ(1−40) in aqueous solution] suggest that there is strong association of Aβ(1−40) with SDS micelles and that the structures derived here reflect a micelle-bound state. This is consistent with previous studies which have confirmed association of Aβ(1−40) with negatively charged vesicles *(30)* and of shorter Aβ fragments with SDS micelles

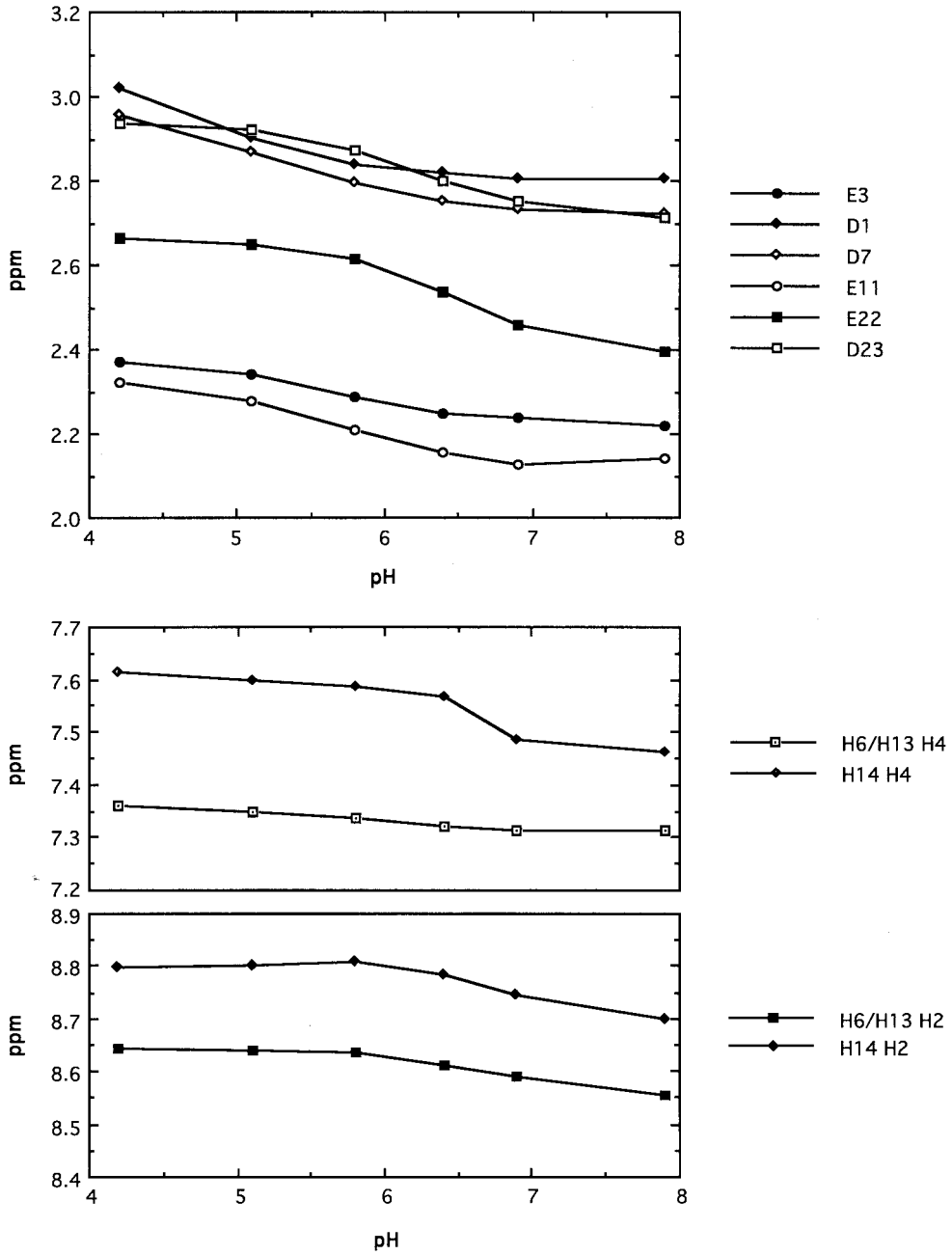

FIGURE 10: Changes in side chain chemical shifts with pH. The upper panel shows the chemical shift of the β-protons of residues with carboxyl side chains at the pH values given in Figure 9. For clarity, the average of the two β-proton chemical shifts is shown. The lower panels show the protons of the indole rings of histidine residues (H4 = HD1, H2 = HE1) at the same pH values. The pH behaviors of the side chains of E22 and D23 and of the H4 proton of H14 are clearly different to other residues of similar type.

(29). While the oligomeric state of Aβ(1−40) in our sample cannot be ascertained with certainty, it is likely to be monomeric, with one Aβ(1−40) molecule per micelle. Garzon-Rodriguez et al. *(31)* recently reported the existence of a stable Aβ(1−40) dimer, but this was under markedly different solution conditions (no SDS) and a β-structure was suggested for the dimer. We clearly observe helical regions within Aβ(1−40) and do not detect any intermolecular NOEs that might indicate dimeric species. These observations reinforce the emerging view that the structure and oligomeric state of Aβ(1−40) are very sensitive to the solution environment.

Comparisons with Other Structural Studies. There have been two previous reports of markedly different solution structures of Aβ(1−40). Using CD spectroscopy *(30)*, Aβ(1−40) was found to associate with negatively charged phospholipid vesicles at pH 7.4 in various buffers (Tris, Mops, and phosphate) to form a β-sheet, a finding in conflict with our results. While our structures were calculated based on data acquired at pH 5.1, at the highest pH tested in the present study (7.9) the structure retains some helicity, particularly in helix 2, as assessed by chemical shift data. It is also clear from differences between αH chemical shifts and random-coil values, as well as qualitative analysis of NOE connectivities, that the structure tends toward random-coil rather than a β-sheet as the pH is increased up to 7.9. This is illustrated, for example, in Figure 10 for H14, where the positive $\Delta\delta_{H\alpha}$ decreases with increasing pH. The differences between the described CD structure and the current NMR structure may be due to the effects of vesicles

versus micelles, or to the mode of interaction of the peptide with the micelle or vesicle surface.

A previous NMR solution structure of Aβ(1−40) in 40% aqueous TFE at pH 2.8 *(32)* contained two helices between residues 15−23 and 31−35, the rest of the peptide assuming a random-coil conformation. This structure is in general agreement with our result of two separate C-terminal helices. The break in the helix involves residues (G25 and S26) known as helix breakers and specifically predicted to be so for this sequence *(32)*. The fact that the break is experimentally detected in two different solvents confirms that it is dependent on factors intrinsic to the sequence rather than reflecting effects due to a micelle boundary.

The Aβ(1−28) fragment has been studied by NMR spectroscopy in aqueous solution and in 60% aqueous TFE *(33)*. In aqueous solution, the peptide was found to be a random-coil structure over the pH range 1−4 and precipitated in the range 4−7 presumably due to formation of a β-sheet aggregated structure. In 60% TFE, the peptide is reported to be α-helical at pH 1−4. At the lowest pH studied (pH 1), the helix extended over most of the sequence. At higher pH, residues 2−7 were essentially random-coil, and the helix apparently persisted over residues 10−27. The similarity to this study lies only in the observed trend for helical content to increase with decreasing pH. Talafous et al. *(34)* found that in aqueous SDS solution at pH 3.0 the Aβ(1−28) fragment consisted of two helices, 2−11 and 13−27, separated by a bend centered on residue 12. The finding of the N-terminal helical region is in contrast to the results presented here, although it is possible that the differences observed may be due to the differences in pH. Zagorski and Barrow *(33)* have previously suggested that the pH dependence of the helicity of Aβ peptides may be due to the presence of several negatively charged residues (D7, E11, and E22) on the same helical face. The formation of a helix over the N-terminal region would bring the side chains of D7 and E11 into close proximity and would therefore be disfavored at high pH where these side chains would be charged.

Another NMR study by Lee et al. *(14)* examined Aβ(1−28) in aqueous solution at pH 2.1 and 5.6 by NMR at submillimolar concentrations. The peptide adopted a predominantly random-coil structure at both pH values. In DMSO, Aβ(1−28) has been shown to have some limited helical structure *(35)*. Thus, Aβ(1−28) is least helical in water or DMSO, and most helical in aqueous TFE and SDS micelle solutions. Although this is not surprising given the nature of the solvents, it is notable that in both DMSO and aqueous SDS the amount of helix observed for Aβ(1−28) was higher than observed in this study for Aβ(1−40) under similar conditions. It is possible that Aβ(1−28) has an inherently higher helical propensity than Aβ(1−40).

Lee et al. *(14)* also studied the Aβ(10−35)NH_2 fragment under conditions similar to those used for Aβ(1−28). It was suggested that a pH-dependent conformational transition occurred from an unstructured conformation at low pH to a conformation containing turns or strands at higher pH. That study contrasts with previous work in TFE or SDS solutions, including the present results, where helical conformers were detected at low pH. However, their data for Aβ(10−35)-NH_2 at pH 5.6 in aqueous solution indicate a large number of sequential NH−NH NOE connectivities and some small $^3J_{H\alpha-NH}$ coupling constants over residues 10−30, consistent with at least nascent helicity. The data for Aβ(10−35)NH_2 are contrary to those for longer fragments since this peptide appears to increase in helicity with increasing pH. These results cast doubt on the relevance of Aβ(10−35)NH_2 as a model for longer Aβ peptides.

Very recently the solution structure of Aβ(12−28) in SDS micelles was reported *(29)* to be helical between residues 16 and 24, in agreement with one side of our broken helix in Aβ(1−40). Also, conformational changes were detected for Aβ(12−28) as a function of pH and lipid type, SDS micelles strongly favoring the observed helicity. The pH-dependent conformational changes were attributed to protonation/deprotonation of the side chains of H13, H14, E22, and D23 and resultant alterations in the interaction between the peptide and micelles. These results agree very well with those reported here for Aβ(1−40).

Implications of the Calculated Structure. The production of Aβ peptides requires proteolytic cleavage of APP by β- and γ-secretases, as shown in Figure 11. Inhibitors of β- and/or γ-secretase could in principle decrease circulating Aβ concentrations, so these secretases are potential targets for drug design. APP is also processed via another, nonamyloidogenic pathway in which it is cleaved between Q15 and K16 of the Aβ sequence by a third enzyme, α-secretase. We recently reported that proteases of all the major classes (serine, aspartic, metallo, and cysteine proteases) recognize their inhibitors/substrates only in extended conformations *(36, 37)*, so the structure of Aβ(1−40) in the regions around the three secretase cleavage sites is therefore of particular interest, as are conformational transitions that facilitate cleavage or aggregation.

The location of the membrane-spanning region of APP is also important in understanding the action of secretases. It is commonly stated that residues 1−28, corresponding to Aβ-(1−28), form the extracellular domain, while 29−40 are within the membrane-spanning region of APP (Figure 11a). However, this assertion appears to be largely based on theoretical grounds (hydrophobicity) and on the location of a hydrophilic lysine triplet signature commencing at residue 53, with the predicted intracellular membrane boundary being at residues 52−53 *(16)*. There seems to be little direct experimental evidence to prove this membrane location. Although Aβ(1−40) may adopt quite a different conformation from the corresponding region in intact APP, the structures derived here at least provide an experimental starting point for deducing the likely membrane-spanning domain of APP. Three possible models (Figure 11a,b,c) for the location of the transmembrane domain of APP are discussed based upon our data and other recent results.

The first possibility (Figure 11a), corresponding to the conventional view *(16)*, is that residues 1−28 are extracellular and residues 29−40 are located in the cell membrane. This is consistent with the conformation calculated here if our helix 2 is inserted in the membrane and the extracellular or water/lipid boundary lies at the kink between helices. In this model, the accepted boundary prediction of 52−53 *(16)* places a triplet of lysine residues in the cytoplasm immediately adjacent to the membrane, as is common in membrane-anchored proteins, but leaves the γ-secretase cleavage site buried deep within the membrane. In Aβ(1−40), residues 28−36 are helical, and this is likely to be

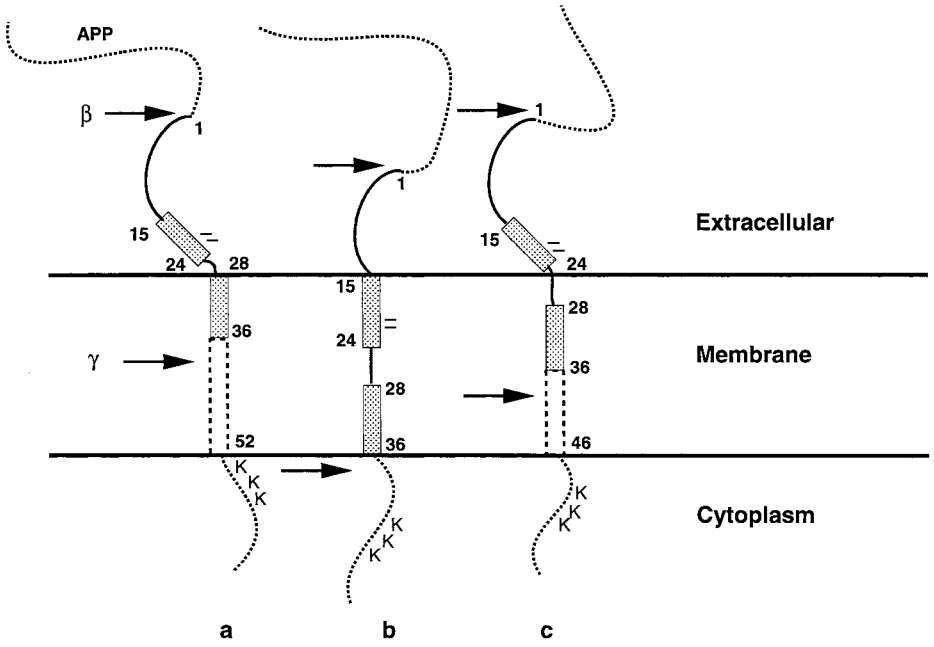

FIGURE 11: Possible models for the association of APP with membranes based on structural findings for Aβ(1−40). Selected residues are numbered based on the sequence of Aβ(1−40). The two experimentally determined helices are indicated by stippled rectangles. The dashed rectangles indicate regions that either are disordered or are beyond the C-terminus of Aβ(1−40) but likely to be within the membrane. The negative charges for Glu22 and Asp23 are indicated, and the β- and γ-secretase cleavage sites are arrowed. (a) indicates the currently accepted model for insertion of APP into the membrane. This model was based on the hydrophobicity profile of APP and is consistent with the location of a triplet of lysine residues at positions 53−55, which may anchor APP to the membrane. Model (b) applies to the case where APP is pushed further through the membrane into the cell, thus incorporating the entire known helical domains of Aβ(1−40) within the membrane. This model also places known secretase cleavage sites at the membrane boundaries. In model (c), the position of Aβ(1−40) is intermediate between those in (a) and (b). This places the C-terminus at a location consistent with recent experimental evidence of Tischer and Cordell (*38*).

maintained for APP. In APP, the structure of residues 37−52 is unknown, but is likely to be helical. The number of residues within the membrane in this model (24, inclusive of residues 29 and 52) is in the range expected for transmembrane helices *(17)*. The functional role, if any, of extracellular helix 1 in this model is open to question.

The second possibility (Figure 11b) is that the entire helical region of Aβ(1−40) (residues ∼15−36) forms the membrane-spanning region of this peptide and its precursor APP. The α-secretase cleavage site (residues 16−17) would as a consequence be located at or near the water−lipid interface, and the γ-secretase site would be exposed near the cytoplasmic membrane boundary. Based on the experimentally determined helix termini at residues 15 and 36 in Aβ(1−40), the membrane-spanning domain would be 22 residues. The slightly smaller number of residues required to span the membrane compared to the previous model is consistent with a break in the compact helical structure at residues 25−27. Against this model is the location in the membrane of potentially negatively charged residues (E22, D23) which normally prevent membrane insertion *(38)*.

The third model (Figure 11c) involves placing the membrane boundary immediately on the C-terminal side of helix 1 which contains charged residues E22 and D23. In APPs, the transmembrane domain would then comprise residues 25−46, based on a 22 residue membrane span, which, as in model 2 above, reflects the lack of compact helical structure for residues 25−27. The close proximity of residues 22 and 23 to the charged headgroups of the surfactant could then explain the anomalously high pK_a of their side chain carboxyls. This model is also consistent with the amphipathic nature of helix 1.

This third alternative for the C-terminal boundary of the transmembrane domain is appealing for a number of reasons. First, a recent study of APP *(38)* indeed suggested that the cytoplasmic membrane boundary is between residues 46−47 rather than the generally accepted boundary at 52−53 *(16)*. Second, key mutations in APPs that are associated with AD and related diseases *(39)* occur at residues (i.e., 21, 22, 46) that are now exposed to solvent and accessible to proteases. For example mutations of residue 46 are known to alter the cleavage site of APP that exposes the C-terminus of Aβ *(38)*. Third, exposure of these charged residues may be important for interaction with pathological chaperones such as apolipoprotein (ApoE), which is known to bind tightly in a pH-dependent manner to Aβ(1−40) in cerebrospinal fluid *(40)*.

Consistent with the C-terminal half of the Aβ region of APP being inserted in lipid or membrane, the isolated fragment Aβ(25−35) is known to insert into the membrane of liposomes *(41)*, and the NMR structure of Aβ(25−35) is helical in LiDS micelles *(42)*. Also, Aβ(1−40) itself can incorporate into membrane bilayers and form ion channels in model cell membranes. Indeed, there have been a number of reports that the neurotoxicity of Aβ is due to formation of cation-selective ion channels in neuronal membranes *(43−45)*. In principle, isolated Aβ peptides may interact with membranes in the same way as illustrated in Figure 11 for APP. However, in the absence of the remainder of the APP protein sequence, different modes of interaction of isolated Aβ peptides with membranes are also possible. Different modes of interaction are indeed quite likely if Aβ peptides do function as ion channels as this would necessarily involve an association between multiple Aβ(1−40) peptides to form

a pore in the membrane.

Durell et al. *(46)* have modeled several potential channels that might be formed by Aβ based on a secondary structure prediction for monomeric units in a membrane environment. The predicted structure of the monomeric Aβ(1−40) unit involves a hairpin region from 3 to 13, a helix from 16 to 24, a kink at 25−27, and a second helix between residues 28 and 40. Several possible modes of association of these monomers to form ion channels were described although none is yet proven. Our experimental data provide support for the possibility of Aβ forming ion channels of the type modeled. The helical regions of our structures agree remarkably well with the secondary structure predicted by Durell et al. *(46)*. In the modeled ion channels, helix 1 lies parallel to the membrane plane, and its amphipathic nature favors interaction with the membrane surface. This type of interaction is suggested from our data by the raised pK_a values of E22 and D23 of Aβ(1−40) in aqueous SDS micelles.

We also note that the properties of the helix−hinge−helix region identified for Aβ(1−40) are similar to those of helix−loop−helix regions found in the membrane-inserting protein diphtheria toxin *(47)*. In the latter case, low pH (<4) stabilizes acidic amino acid side chains near the hinge like Asp and Glu in a protonated (uncharged) and membrane-soluble form while higher pH (>5.5) leads to their deprotonation and results in a highly charged and water-soluble form that is unable to penetrate membranes. These similarities again raise the prospect of a membrane-inserting potential for Aβ(1−40). The average interaxial angle defining the hinge ($\theta = 48°$) in the Aβ(1−40) peptide is similar to that found in the well-known membrane-inserting peptide melittin ($\theta = 49°$), but different from that in other proline-kinked helices reported in proteins ($26 \pm 5°$) *(27)*.

A final interesting feature of the calculated structure is the presence of a number of glycine residues in helix 2. A pattern of glycines spaced four residues apart stretches from G29 to G37. This spacing means that the glycine residues occupy one side of the helix and the backbone atoms in this region are more highly exposed to solvent than is normally expected of helices. This may be relevant to the recognition of the peptide by γ-secretase which cleaves the C-terminus of the Aβ peptides to the C-terminal side of the 28−36 helix. The ion channel model of Durell et al. *(46)* also predicted the observed glycine pattern.

In conclusion, this study has definitively established that Aβ(1−40) exists in a water−micelle medium as a random coil from residues 1 to 14, as separate α-helices from 15 to 24 and from 28 to 36, and as a hinge or kinked region at 25−27. The structure is consistent with NMR results for the fragments Aβ(12−28) *(29)* and Aβ(25−35) *(42)* in micelle environments. The conformational transition from α-helix to random coil with increasing pH, the pH-dependent chemical shifts of E22 and D23, and the onset of aggregation observed for random-coil Aβ(1−40) in water alone are consistent with a helix−coil−sheet progression prior to aggregation. The helix−hinge−helix and pH-dependent conformational changes detected are reminiscent of membrane-inserting pore-forming proteins *(47)* and may be relevant to the reported membrane-inserting and ion-channel properties of Aβ(1−40) *(43−45)*. Finally, the location of the micelle boundary, as suggested in these NMR experiments by the helical domains of Aβ(1−40), is consistent with new evidence for an alternative location of the cellular membrane-spanning domain of APPs, namely, at approximately residues 25−46 *(38)*. Further studies of such peptide−micelle and peptide−membrane interactions are needed.

REFERENCES

1. Iverson, L. L., Mortishire-Smith, R. J., Pollack, S. J., and Shearman, M. S. (1995) *Biochem. J. 311*, 1−16.
2. Masters, C. L., Simms, G., Weinman, N. A., Multhaup, G., McDonald, B. L., and Beyreuther, K. (1985) *Proc. Natl. Acad. Sci. U.S.A. 82*, 4245−4249.
3. Mattson, M. P. (1997) *Phys. Rev. 77*, 1081−1132.
4. Selkoe, D. J. (1993) *Trends Neurosci. 16*, 403−409.
5. Mattson, M. P. (1995) *Nat. Struct. Biol. 2*, 926−928.
6. Lorenzo, A., and Yankner, B. A. (1994) *Proc. Natl. Acad. Sci. U.S.A.* 91, 12243−12247.
7. Simmons, L. K., May, P. C., Tomaselli, K. J., Rydel, R. E., Fuson, K. S., Brigham, E. F., Wright, S., Lieberburg, I., Becker, G. W., Brems, D. N., and Li, W. Y. (1994) *Mol. Pharmacol. 45*, 373−379.
8. Pike, C. J., Walencewicz-Wasserman, A. J., Kosmoski, J., Cribbs, D. H., Glabe, C. G., and Cotman, C. W. (1995) *J. Neurochem. 64*, 253−265.
9. Haass, C., Schlossmacher, M. G., Hung, A. Y., Vigo-Pelfrey, C., Mellon, A., Ostaszewski, B. L., Lieberburg, I., Koo, E. H., Schenk, D., Teplow, D. B., and Selkoe, D. J. (1992) *Nature 359*, 322−325.
10. Seubert, P., Vigo-Pelfrey, C., Esch, F., Lee, M., Dovey, H., Davis, D., Sinha, S., Schlossmacher, M. G., Whaley, J., Swindlehurst, C., McCormack, R., Wolfert, R., Selkoe, D. J., Lieberburg, I., and Schenk, D. (1992) *Nature 359*, 325−327.
11. Iwatsubu, T., Odaka, A., Suzuki, N., Mizusawa, H., Nukina, N., and Ihara, Y. (1994) *Neuron 13*, 45−53.
12. Jarrett, J. T., Berger, E. P., and Lansbury, P. T., Jr. (1993) *Biochemistry 32*, 4693−4697.
13. Yankner, B. A., Duffy, L. K., and Kirschner, D. A. (1990) *Science* 250, 279−282.
14. Lee, J. P., Stimson, E. R., Ghilardi, J. R., Mantyh, P. W., Lu, Y.-A., Felix, A. M., Llanos, W., Behbin, A., Cummings, M., Van Criekinge, M., Timms, W., and Maggio, J. E. (1995) *Biochemistry 34*, 5191−5200.
15. Burdick, D., Soreghan, B., Kwon, M., Kosmoski, J., Knauer, M., Henschen, A., Yates, J., Cotman, C., and Glabe, C. (1992) *J. Biol. Chem. 267*, 546−554.
16. Kang, J., Lemaire, H.-G., Unterbeck, A., Salbaum, J. M., Masters, C. L., Grzeschik, K.-H., Multhaup, G., Beyreuther, K., and Müller-Hill, B. (1987) *Nature (London) 325*, 733−736.
17. Henry, G. D., and Sykes, B. D. (1994) *Methods Enzymol. 239*, 515−535.
18. Schnölzer, M., Alewood, P., Jones, A., Alewood, D., and Kent, S. B. H. (1992) *Int. J. Pept. Protein Res. 40*, 180−193.
19. Jeener, J., Meier, B. H., Bachmann, P., and Ernst, R. R. (1979) *J. Chem. Phys. 71*, 4546−4553.
20. Braünschweiler, L., and Ernst, R. R. (1983) *J. Magn. Reson. 53*, 521−528.
21. Rance, M., Sørenson, O. W., Bodenhausen, G., Wagner, G., Ernst, R. R., and Wüthrich, K. (1983) *Biochem. Biophys. Res. Commun. 177*, 479−495.
22. Marion, D., and Wüthrich, K. (1983) *Biochem. Biophys. Res Commun. 113*, 967−974.
23. Piotto, M., Saudek, V., and Sklenar, V. (1992) *J. Biomol. NMR 2*, 661−665.
24. Wishart, D. S., Bigam, C. G., Yao, J., Abildgaard, F., Dyson, H. J., Oldfield, E., Markley, J. L., and Sykes, B. D. (1995) *J. Biomol. NMR 6*, 135−140.
25. Brünger, A. T. (1992) XPLOR version 3.0 Manual, Yale University, New Haven, CT.
26. McLeish, M. J., Nielsen, K. J., Najbar, L. V., Wade, J. D., Lin, F., Doughty, M. B., and Craik, D. J. (1994) *Biochemistry, 33*, 11174−11183.

27. Barlow, D. J., and Thornton, J. M. (1988) *J. Mol. Biol. 201*, 601−619.
28. Wang G. S., Treleaven, W. D., and Cushley, R. J. (1996) *Biochim. Biophys. Acta 1301*, 174−184.
29. Fletcher, T. G., and Keire, D. A. (1997) *Protein Sci. 6*, 666−675.
30. Terzi, E., Hölzemann, G., and Seelig, J. (1995) *J. Mol. Biol. 252*, 633−642.
31. Garzon-Rodriguez, W., Sepulveda-Becerra, M., Milton, S., and Glabe, C. G. (1997) *J. Biol. Chem. 272*, 21037−21044.
32. Sticht, H., Bayer, P., Willbold, D., Dames, S., Hilbich, C., Beyreuther, K., Frank, R. W., & Rösch, P. (1995) *Eur. J. Biochem. 233*, 293−298.
33. Zagorski, M. G., and Barrow, C. J. (1992) *Biochemistry 31*, 5621−5631.
34. Talafous, J., Marcinowski, K. J., Klopman, G., and Zagorski, M. G. (1994) *Biochemistry 33*, 7788−7796.
35. Sorimachi, K., and Craik, D. J. (1994) *Eur. J. Biochem. 219*, 237−251.
36. Reid, R. C., and Fairlie, D. P. (1997) *Adv. Amino Acid Mimetics Peptidomimetics 1*, 77−107.
37. Fairlie, D. P., West, M. L., and Wong, A. K. (1998) *Curr. Med. Chem. 5*, 29−62.
38. Tischer, E., and Cordell, B. (1996) *J. Biol. Chem. 271*, 21914−21919.
39. Hendriks, L., and Van Broeckhoven, C. (1996) *Eur. J. Biochem. 237*, 6−15.
40. Strittmatter, W. J., Weisgraber, K. H., Huang, D. Y., Dong, L.-M., Salvesen, G. S., Pericak-Vance, M., Schmechel, D., Saunders, A. M., Goldgaber, D., and Roses, A. D. (1993) *Proc. Natl. Acad. Sci. U.S.A.* 90, 8098−8102.
41. Mason, R. P., Estermyer, J. D., Kelly, J. F., and Mason, P. E. (1996) *Biochem. Biophys. Res. Commun. 222*, 78−82.
42. Kohno, T., Kobayashi, K., Maeda, T., Sato, K., and Takashima, A. (1996) *Biochemistry 35*, 16094−16104.
43. Arispe, N., Pollard, H. B., and Rojas, E. (1993a) *Proc. Natl. Acad. Sci. U.S.A.* 90, 10573−10577.
44. Arispe, N., Rojas, E., and Pollard, H. B. (1993b) *Proc. Natl. Acad. Sci. U.S.A.* 90, 567−571.
45. Kawahara, M., Arispe, N., Kuroda, Y., and Rojas E. (1997) *Biophys. J. 73*, 67−75.
46. Durell, S. R., Guy, H. R., Arispe, N., Rojas, E., and Pollard, H. B. (1994) *Biophys. J. 67*, 2137−2145.
47. Bennett, M. J., and Eisenberg, D. (1994) *Protein Sci. 3*, 1464−1475.
48. Andersen, N. H., Cort, J., Harris, S. M., Lee, G. M., Liu, Z., and Neidigh, J. (1996) 37th ENC, Asilomar, CA.
49. Barrow, C. J., and Zagorski, M. G. (1991) *Science 253*, 179−182.
50. Jayawickrama, D., Zink, S., Vandervelde, D., Effiong, R. I., and Larive, C. K. (1995) *J. Biomol. Struct. Dynam. 13*, 229−244.

BI972979F